RESEARCH ARTICLE

Cortico-muscular coherence of time–frequency and spatial characteristics under movement observation, movement execution, and movement imagery

Lu Zhou[1] · Biao Wu[2] · Bing Qin[1] · Fan Gao[1] · Weitao Li[1] · Haixu Hu[3] · Qiaoqiao Zhu[1] · Zhiyu Qian[1]

Abstract

Studies show that movement observation (MO), movement imagery (MI), or movement execution (ME) based brain–computer interface systems are promising in promoting the rehabilitation and reorganization of damaged motor function. This study was aimed to explore and compare the motor function rehabilitation mechanism among MO, MI, and ME. 64-channel electroencephalogram and 4-channel electromyogram data were collected from 39 healthy participants (25 males, 14 females; 18–23 years old) during MO, ME, and MI. We analyzed and compared the inter-cortical, inter-muscular, cortico-muscular, and spatial coherence under MO, ME, and MI. Under MO, ME, and MI, cortico-muscular coherence was strongest at the beta-lh band, which means the beta frequency band for cortical signals and the lh frequency band for muscular signals. 56.25–96.88% of the coherence coefficients were significantly larger than 0.5 ($ps < 0.05$) at the beta-lh band. MO and ME had a contralateral advantage in the spatial coherence between cortex and muscle, while MI had an ipsilateral advantage in the spatial coherence between cortex and muscle. Our results show that the cortico-muscular beta-lh band plays a critical role in the synchronous coupling between cortex and muscle. Also, our findings suggest that the primary motor cortex (M1), dorsolateral prefrontal cortex (DLPFC), supplementary motor area (SMA), and premotor cortex (PMC) are the specific regions of MO, ME, and MI. However, their pathways of regulating muscles are different under MO, ME, and MI. This study is important for better understanding the motor function rehabilitation mechanism in MO, MI, and ME.

Keywords Electroencephalography (EEG) · Movement observation (MO) · Movement execution (ME) · Movement imagery (MI) · Cortico-muscular coherence

✉ Qiaoqiao Zhu
zqq@nuaa.edu.cn

✉ Zhiyu Qian
zhiyu_q@163.com

[1] Department of Biomedical Engineering, Nanjing University of Aeronautics and Astronautics, 29 Jiangjun Avenue, Jiangning District, Nanjing 211100, Jiangsu, China

[2] Electronic Information Department, Nanjing University of Aeronautics and Astronautics, Nanjing, China

[3] Sports Training Academy, Nanjing Sport Institute, Nanjing, China

Introduction

Stroke is a major cause of disability in adults and the second leading cause of death worldwide (Baccetto and Lehmann 2019), causing 5.5 million death directly or from stroke complications per year (Naghavi et al. 2017). Statistics predict that by 2030, this number will reach 12 million per year (Feigin et al. 2014). For those stroke survivors, about 85% suffer from severe motor dysfunction, disabling them from taking care of themselves and living a quality life (Hatem et al. 2016). Rehabilitation training is effective in restoring motor function to patients (Hatem et al. 2016).

Traditional motor rehabilitation methods are mainly through taking drugs (Luo et al. 2017), physical therapy (Garcia-Cabo and Lopez-Cancio 2020), and occupational

therapy (Andrews et al. 2021). These methods are not effective in engaging subjective motor intention, resulting in slow progress in motor recovery. With the development of neuroimaging technology, researchers developed neural feedback training based on electroencephalogram (EEG) as an active intervention for motor function rehabilitation. Numerous studies showed that a brain-computer interface (BCI) system based on movement observation (MO), movement imagery (MI), or movement execution (ME) can effectively improve stroke patients' motor abilities, cognitive abilities, and the activation effect of their damaged nerves (Foong et al. 2019; Sakurada et al. 2017; Signal et al. 2020). Ono et al. found that MO, MI, and proprioceptive feedback could effectively regulate brain sensorimotor rhythm response (Ono et al. 2018). Ander et al. and Kleim et al. found that MI-BCI-controlled mechanical correction equipment can effectively improve the motor function of stroke patients (Kleim and Jones 2008; Ramos-Murguialday et al. 2013). Garrison et al. reported that MO could activate specific motor cortices in damaged motor circuits after stroke (Garrison et al. 2013). Neuroimaging studies found that MI activates similar cortices as those activated by ME (Guillot et al. 2008; Mizuguchi et al. 2017). The repetitive training based on MI or MO can activate the specific cortex for regaining relevant motor functions. However, this training cannot fully activate and synergize various sensory pathways simultaneously.

The BCI system with multi-channel functional electrical stimulation (FES) controlled by EEG can activate the cortex-muscle synchronously, strengthen the activation of the sensorimotor cortex, and promote the repair and reorganization of damaged nerve function (Qiu et al. 2016; Zhao et al. 2016; Zulauf-Czaja et al. 2021). Zhang et al. found a strong EEG-EMG coherence at the beginning of the ME (Zhang et al. 2021). Krauth et al. proposed that the EEG-EMG coherence can be a biomarker for motor recovery post-stroke (Krauth et al. 2019).

These studies showed that the BCI-FES system based on MI or MO can realize synchronous coupling between cortex and muscle, promoting the recovery of motor function. However, the motor rehabilitation mechanisms based on MI, MO, and ME are unclear. We projected scalp potential to the cerebral cortex by EEG source imaging (ESI) (Michel and Brunet 2019) and then calculated the coherence between cortical potential and EMG instead of directly calculating the coherence between scalp potential and EMG. In addition, unlike other studies (Kim et al. 2017; Tun et al. 2021) which directly extract motion-related frequency bands through experience, we used power spectral density (PSD) (Hsueh et al. 2015) to select the most active EMG signal frequency band under these tasks. We analyzed and compared the time–frequency and spatial coherence among MI, MO, and ME, which is important for

a better understanding of the motor rehabilitation mechanism.

Materials and methods

Subjects

A total of 39 subjects (25 males, 14 females) aged 18 to 23 participated in this study. All subjects were healthy, with no history of neurological dysfunction, vision problems, upper limb pathology, or abnormal gait. All subjects were right-handed. All subjects gave written informed consent, and the Institutional Ethics Committee of Hunan Cancer Hospital, Hunan, China, approved the study.

Experiment protocol

The experiment included three movement conditions (MO, ME, MI) and two modes (Task, Rest), as seen in Fig. 1. In Task mode, six tasks, including the left fist task under MO (T1), ME (T3), and MI (T5) conditions, and the right fist task under MO (T2), ME (T4), and MI (T6) conditions, were performed.

There were 14 trials in each session under each movement condition, including seven left fist tasks and seven right fist tasks. Each subject underwent three repeated sessions under each movement condition. The order in which the MI, MO, and ME trials appeared was MO, ME, and MI.

After all trials of a movement condition were completed, the subjects rested for half an hour, trying to avoid any effect on the results of the next movement condition. The time intervals for different motor condition tasks have not been standardized in the MO, MI, and ME studies. The experimental paradigm used by Zhang et al. (2019) had time intervals of 30 s and 90 s between MO and ME and between ME and MI, respectively. The experimental paradigm Di Nota et al. (2017) used had a time interval of 15 s between MO and MI. Our time interval is longer than these time intervals, we believe the effect of MI, MO, and ME order on our results may not be insignificant. In total, 4914 trials were carried out. Each trial starts with an instruction showing which condition to perform. Next, in the Rest mode, subjects rest for 5 s before the next task. Under MO condition, a 5 s video clip of holding a left fist or right fist was displayed, and the subject was asked to observe the fist movement without actually holding fists. The hand starts from an open palm position. Then the hand folds into a fist. This movement is repeated three times during the 5 s video clip. Under the ME and MI conditions, a white dot was displayed on the monitor's left or right side for 5 s. Subjects were asked to make a left or right fist or
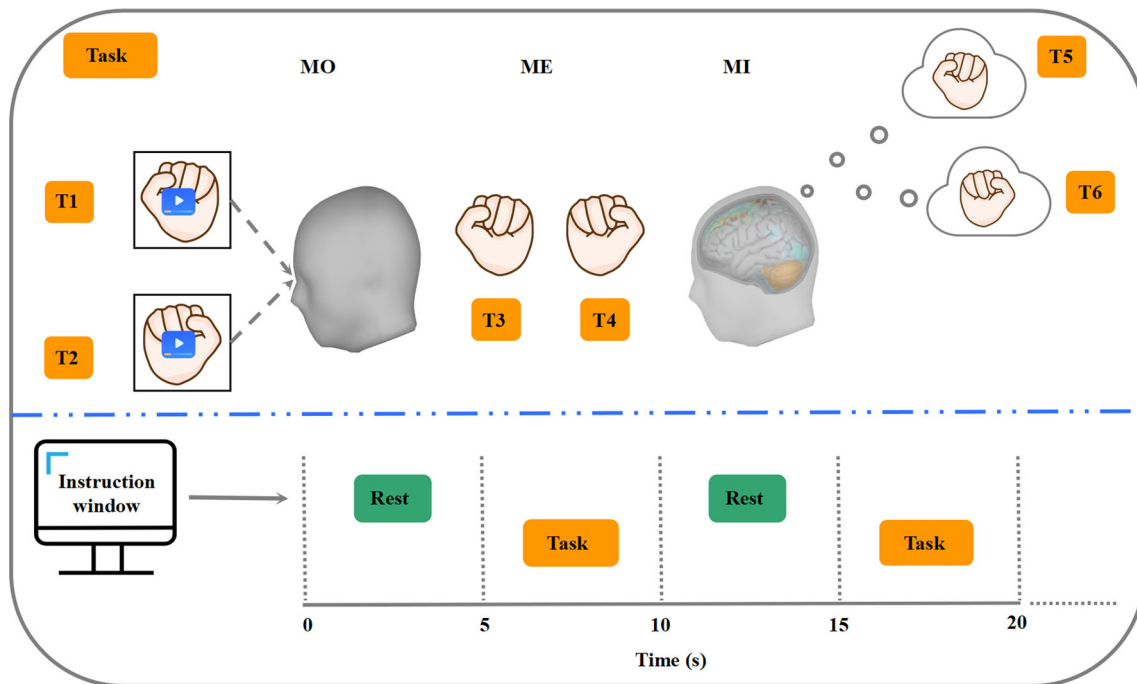
Fig. 1 Schematic representation of the experiments for the left fist (T1, T3, T5) and right fist (T2, T4, T6) tasks under different movement conditions (MO, ME, MI). Each session contains seven left and seven right fist tasks under the same motion condition. Before the start of each session, the display shows an instruction window informing the subject of the motor condition (MO, ME, MI) for the tasks to be performed in that session. There was a 5-s rest period before each task and a 5-s rest period between tasks

imagine making a left or right fist correspondingly at their own pace. The left or right fist trials appeared in a pseudo-random order.

Data acquisition

An eego^{TM}mylab (ANT Neuro, Berlin, Germany) was utilized to simultaneously collect 64-channel EEG signals and 4-channel EMG signals throughout the experiment. The EEG electrodes were placed according to the 10–20 international system. EMG signals of both forearms' flexor carpi ulnaris (FCU) and extensor digitorum (ED) muscles were recorded on the skin surface. A pair of electrodes were placed on the subject's left (B3, B4) and right fore-arms (B1, B2) in a standard belly-tendon montage. The sampling rates of EEG and EMG were set to 1000 Hz.

Data analysis

EEG and EMG pre-processing

Custom programs in MATLAB (MathWorks, Natick, MA, USA) incorporating functions of Brainstorm were applied to conduct data analysis offline (Tadel et al. 2011). The EEG and EMG data were notch filtered using a Butterworth infinite impulse response (IIR) filter to remove 50 Hz and corresponding harmonics electrical noise. They were then band-pass filtered using a finite impulse response (FIR) filter to band-pass 1–50 Hz components.

After filtering, an independent component analysis (ICA) was employed to remove eye movement, eye blink, and custom event artifacts (Gao et al. 2010). Data with abnormality or large noise were excluded based on visual inspection. The exclusion criteria were: (1), signals with large motor defect, (2), loss of signals on certain channels. In total, data of five subjects were excluded accordingly. Finally, the pre-processed EEG and EMG signals were down-sampled to 250 Hz and segmented into 5 s-trials. The signals for segmentation were collected during the MI/MO/ME tasks, in which 5-s stimulation followed by 5-s rest was repeated 14 times, making each session last 140 s. This session was then segmented into 5-s trials, containing 14 motor task-related trials and 14 rest trials.

EEG source estimation

To better analyze the real motor intention of the subjects, ESI was applied to project the scalp potential (**L**, recorded EEG data) to the cerebral cortex (**H**, current densities of sources):

$$L = TH + N \tag{1}$$

where **T** is a matrix of lead field and **N** is a matrix of noise covariance. In our experiment, we used the identity matrix

as the noise matrix, as done in many studies (Dale and Sereno 1993; Liu et al. 1998), and applied weighted minimum norm estimation (WMNE) to compute the matrix of lead field (T).

We used the head model template instead of creating the personalized head model from individual anatomical data. To reduce the error introduced by the head model, we chose the Colin 27 average brain (Collins et al. 1998) with high signal-to-noise ratio and structure definition, and warped the Colin 27 average brain according to the electrode montage worn by the subjects. First, the boundary element method (BEM) was used to compute the shape and conductivity of the warped head, solving the forward problem (von Ellenrieder et al. 2005). Then, we used the dipoles model and the minimum norm imaging method to solve the inverse problem. Minimum norm imaging estimates the amplitude of brain sources at each grid location determined by the forward head model. The number of dipoles (5000) is much larger than the number of electrodes (64), which leads to the EEG inverse problem ill-posed. To solve this problem, we introduced a regularization term X:

$$\min_{H} \parallel TH - L \parallel^2 + X \parallel ZH \parallel^2 \tag{2}$$

where Z is a weighted matrix.

$$\hat{H} = T^T (TT^T + XZ)^{-1} L \tag{3}$$

The Brainstorm software is used to realize the source estimation from EEG.

Regions of interests (ROIs) creation

In this paper, we were interested in the current activities of task-related brain regions, including the primary motor cortex (M1) of the left hemisphere (R1), the M1 of the right hemisphere (R2), the dorsolateral prefrontal cortex (DLPFC) of the left hemisphere (R3), the DLPFC of the right hemisphere (R4), the supplementary motor area (SMA) of the left hemisphere (R5), the SMA of the right hemisphere (R6), the premotor cortex (PMC) of the left hemisphere (R7), and the PMC of the right hemisphere (R8) (Hanakawa et al. 2003). These eight areas in the cerebral cortex were defined as the regions of interest (ROIs) in this study. We selected the ROIs based on the Desikan-Killiany cortical atlas. The ROI selection is achieved with Brainstorm software. The source estimation of ROIs was used for coherence calculation.

Time frequency analysis of EEG and EMG

For each subject, the time–frequency distribution of EEG sources extracted from eight ROIs and EMG signals recorded from the FCU and ED muscles were calculated

using a Morlet wavelet-based time–frequency analysis. The temporal resolution of the wavelet is defined by the full-width at half-maximum (FWHM) of its Gaussian kernel. Originally, the center frequency of the wavelet (f_c) was set to 1 Hz, the time resolution was 3 s, and the wavelength was:

$$\sigma_{t,f_c} = \frac{FWHM_{f_c}}{\sqrt{8\ln(2)}} \tag{4}$$

The length of the wavelet (σ_{t,f_c}) is scaled for the remaining frequency (f) by:

$$\sigma_{t,f} = \frac{\sigma_{t,f_c} f_c}{f} \tag{5}$$

Wavelet coefficients were calculated at 0.5 Hz intervals and convolved with the selected waveform by:

$$\psi_f = \left(\sigma_{t,f}\sqrt{\pi}\right)^{-\frac{1}{2}} e^{\frac{t^2}{2\sigma_{t,f}^2}} e^{2\pi i f_c t}, \tag{6}$$

where i is an imaginary number.

For the remaining 34 subjects, time–frequency analysis in each of the theta (4–8 Hz), alpha (8–13 Hz), and beta (13–29 Hz) frequency bands was carried out on EEG data of the 126 trials from the six tasks. In the time–frequency analysis of EMG signals, usually the theta, alpha, and beta frequency bands were used, just like those of EEG in literature (Tun et al. 2021). However, these frequency bands in EMG signals do not have the same physiological meaning as those in EEG signals. Cortical muscle coherence studies usually use the same frequencies (Gao et al. 2018; Tuncel et al. 2010). However, the frequency bands associated with meaningful muscle activation in EMG signals may differ from those in EEG signals under the same task. Usually, the task-relevant frequency band in the EMG signal is selected by band analysis (e.g., power spectral density applied in this paper) (Politti et al. 2016) rather than a specific frequency band (e.g., alpha, beta bands commonly used for EEG).

Here, in this study, we defined a new frequency band, called lh band, which is a leading (l) frequency band for muscles under the six tasks in this study and is a high (h) frequency band. This lh band is related to activation status of the motor tasks, which is related to the high-power spectral density in the EMG signals. The lh frequency band is selected based on the power spectral density (PSD) of the 4-channel EMG signals.

First, the power spectral density (PSD) of the 4-channel EMG signals was calculated and averaged across subjects. Then, based on the results of PSD, the frequency corresponding to the maximum energy density (f_{Max}) and the frequency corresponding to half of the maximum energy density (f_{Hi}, could have multiple values) were found. The two frequencies f_{Hi} closest to f_{Max} {defined as (f_{Hl}, f_{Hh})}

were chosen and consists of a target frequency band (f_{Hl}–f_{Hh}), in which the muscle activities were relatively more active. For each task, a target frequency band were defined this way. For the six tasks, in total we defined six target frequency bands, the overlap among which was defined as our lh band.

According to the results of PSD, the lh frequency band of interest was defined as 30–100 Hz. Time–frequency analysis at theta, alpha, beta, and lh frequency bands were carried out on EMG data. We calculated the average energy density across time to evaluate EEG and EMG wave activity in different frequency bands under each task. We used the average energy (AE) of neuron activity in the cortex and the AE of electrical activity on the muscle surface to measure the level of activation in the cerebral cortex and quantify the degree of muscle activation, respectively.

Coherence analysis

The synchronous changes between EEG of ROIs, EMG of interested muscles, and EEG and EMG under the same task were analyzed through coherence analysis over the 5-s trials. Neuronal electrical signals of eight cortical regions and four muscle surface electrical signals were used for coherence analysis. For a given two signals (x_1, x_2), the coherence was calculated using magnitude-squared coherence as:

$$C_{x1,x2}(f) = \frac{\left|P_{x1,x2}(f)\right|^2}{\left|P_{x1}(f)\right| \times \left|P_{x2}(f)\right|} \tag{7}$$

where $P_{x1}(f)$, $P_{x2}(f)$ are the power spectra of x_1 and x_2, and $P_{x1,x2}(f)$ the cross-power spectra of of x_1 and x_2, at frequency f.

The inter-cortical (EEG-EEG) coherence analysis was carried out on the time–frequency spectrum of three frequency bands (theta, alpha, beta) of eight ROIs to select the brain regions with significant coherence under each task. There were 28 coherence coefficients among eight ROIs for each task and each frequency band.

For inter-muscular (EMG-EMG) coherence analysis, the muscles with higher coherence under the same task were obtained by computing coherence between the time–frequency spectrum of EMG signals on four muscles (left FCU, right FCU, left ED, right ED). Most studies in the literature usually used theta, beta, and alpha waves in EMG signals (Maso et al. 2017; Tun et al. 2021), but we did not use these frequency bands directly. Instead, we selected the active lh band. In order to verify the effectiveness of the lh band, we also calculated the coherence among muscles at theta, alpha, and beta frequency bands. Then we compared the coherence among muscles at the four frequency bands.

There were six coherence coefficients among four muscles for each task and each frequency band.

In cortico-muscular (EEG-EMG) coherence analysis, we calculated the coherence between the EEG time–frequency spectrum at each frequency band (theta, alpha, beta) and the EMG time–frequency spectrum at each frequency band (lh, theta, alpha, beta). The cortico-muscular coherence was calculated for each of the eight ROIs and four muscles, respectively, to analyze the time–frequency coherence and spatial coherence between EEG and EMG.

This study has six cortico-muscular bands, including three different cortico-muscular bands and three same cortico-muscular bands. In different cortico-muscular bands, the frequency band of the cortex is different from that of muscle, including cortico-muscular theta-lh, alpha-lh, and beta-lh bands. In the same cortico-muscular bands, the frequency band of the cortex is the same as that of muscle, including cortico-muscular theta-theta, alpha-alpha, and beta-beta bands. There were 32 coherence coefficients among eight ROIs and four muscles in each cortico-muscular band for each task. The coherence value significance level (C_s) at a particular frequency (Halliday et al. 1995) was determined by:

$$C_s = 1 - (1 - \alpha)^{\frac{1}{M-1}} \tag{8}$$

where α is a confidence interval and set to 0.99 (Muthuraman et al. 2018), M is the number of data segments used in the coherence calculation. The coherence coefficient larger than C_s was defined as that there is synchronous coupling. In this paper, C_s was 0.5.

Statistical analysis

All statistical analyses were performed in IBM SPSS Statistics (Version 26.0.0.0). Paired t-tests were used to investigate whether significant changes in AE values exist in different brain regions/muscles/frequency bands, respectively. The differences in AE values among different brain regions were calculated separately. Similar operations were performed for significant changes in AE values across muscles/frequency bands.

A non-parametric Kolmogorov–Smirnov test was used to test the inter-cortical, inter-muscular, cortico-muscular coherence coefficients for normal distribution. A Levene's test was used for equality of variances. A three-way analysis of variance (ANOVA) was used to verify the significance of the differences in the inter-cortical, inter-muscular, cortico-muscular coherence coefficients at different modes. For inter-cortical coherence statistical analysis, $7 \times 3 \times 28$ ANOVA with the factors Mode (T1, T2, T3, T4, T5, T6, Rest), Frequency (theta, alpha, beta), and Cortical pair (R1–R2, R1–R3, R1–R4, R1–R5, R1–R6, R1–

R7, R1–R8, R2–R3, R2–R4, R2–R5, R2–R6, R2–R7, R2–R8, R3–R4, R3–R5, R3–R6, R3–R7, R3–R8, R4–R5, R4–R6, R4–R7, R4–R8, R5–R6, R5–R7, R5–R8, R6–R7, R6–R8, R7–R8) was used. For inter-muscular coherence statistical analysis, $7 \times 4 \times 6$ ANOVA with the factors Mode (T1, T2, T3, T4, T5, T6, Rest), Frequency (lh, theta, alpha, beta), and Muscle pair (B1-B2, B1-B3, B1-B4, B2-B3, B2-B4, B3-B4) was used. For cortico-muscular coherence statistical analysis, $7 \times 6 \times 32$ ANOVA with the factors Mode (T1, T2, T3, T4, T5, T6, Rest), Frequency (cortico-muscular theta-lh, alpha-lh, beta-lh, theta-theta, alpha-alpha, beta-beta bands), and Cortical muscle pair (R1-B1, R1-B2, R1-B3, R1-B4, R2-B1, R2-B2, R2-B3, R2-B4, R3-B1, R3-B2, R3-B3, R3-B4, R4-B1, R4-B2, R4-B3, R4-B4, R5-B1, R5-B2, R5-B3, R5-B4, R6-B1, R6-B2, R6-B3, R6-B4, R7-B1, R7-B2, R7-B3, R7-B4, R8-B1, R8-B2, R8-B3, R8-B4) was used. The violation of sphericity was tested by Mauchly's test ($\alpha = 0.05$). If the probability of the spherical test is smaller than α, the degree of freedom needs to be corrected by Greenhouse–Geisser correction. A Bonferroni correction was applied for all the post hoc tests that involves multiple comparisons and considered significant at $p < 0.05$.

Results

Time–frequency analysis

The time–frequency spectrum of the ROI source estimations averaged from the data of 34 subjects is shown in Fig. 2.

The results showed that during the six tasks (T1, T2, T3, T4, T5, T6), the AE of three frequency bands (theta, alpha, beta) in ROIs of the left hemisphere (R3, R7, R5, R1) were significantly larger ($ps < 0.05$) than those of the right hemisphere (R4, R8, R6, R2). R3 was the active cortex with the largest AE value in the left hemisphere, and R2 in the right hemisphere. For each task, the AE of the alpha band for each cortex was significantly larger ($ps < 0.05$) than that of the theta/beta band. Under T1, the alpha was active in R1, R3, and R7 ($AE_{alpha} > 10 \times 10^{-19}$). Under T2, theta and alpha waves were more significantly active ($ps < 0.05$), with larger AE in R3 and R7 than in other ROIs. Under T3, the theta wave was significantly active in R7. Under T4, alpha was significantly active in R3 and R1. Under T5 and T6, the AE of each cortex at three bands was less than 10×10^{-19}.

For each EMG channel (B1, B2, B3, B4), the time–frequency characteristics of EMG signals at each frequency band (theta, alpha, beta, lh) under each task (T1, T2, T3, T4, T5, T6) were averaged. The averaged time–frequency analysis of EMG is shown in Fig. 3.

When observing or executing left fist tasks (T1, T3), the electrical activities on the surface of FCU and ED muscles in the left forearm were strongest, with maximum AE at the lh band. Under T5, the electrical activities on the surface of FCU and ED muscles in the left forearm were strongest with maximum AE at the beta band, while in the right forearm, they were strongest at the lh band. Under the right-fist related tasks (T2, T4, T6), the FCU and ED muscles of the right forearm were strongly activated at the lh band ($AE_{lh} > 5 \times 10^{-15}$), while the FCU and ED muscles of the left forearm were strongly activated at the beta band ($AE_{beta} > 5 \times 10^{-15}$).

Coherence analysis

The synchronous coupling of cortices at three frequency bands (theta, alpha, beta) under different tasks (T1, T2, T3, T4, T5, T6) is shown in Fig. 4.

The $7 \times 3 \times 28$ ANOVA with the factors Mode, Frequency, and Cortical pair indicated a significant main effect of Mode, the significant main effect of Frequency, the significant main effect of Cortical pair, and significant interaction between each two of the factors, Mode*Frequency, Mode*Cortical pair, Frequency*Cortical pair, and significant interaction between the three factors, shown in Table 1.

Among all tasks, the number of the cortices with significantly synchronous coupling was largest at the beta band, followed by that at the alpha band, and it was smallest at the theta band. For example, under T1, only the R1–R2 cortical pair had coherence coefficients significantly greater than 0.5 at the theta band ($p < 0.05$). The coherence coefficient between most cortices (0.0070 ± 0.0058) was much smaller than 0.5. At alpha and beta bands, more than 50% and 91% of the coherence coefficients were significantly greater than 0.5 ($ps < 0.05$). Under T2, neuron activities were most significantly active at the alpha band, and the number of cortical regions with coherence coefficients significantly greater than 0.5 was the largest among the six tasks, with 75% of the coherence coefficients significantly greater than 0.5. Under T4, the number of synchronously coupled cortices was significantly highest at the beta band compared to those at the theta and alpha bands.

The coherence of four muscles at four frequency bands (lh, theta, alpha, beta) under the six tasks is shown in Fig. 5.

The $7 \times 4 \times 6$ ANOVA with the factors Mode, Frequency, and Muscle pair indicated a significant main effect of Mode, the significant main effect of Frequency, the significant main effect of Muscle pair, and significant interaction between each two of the factors, Mode*Frequency, Mode*Muscle pair, Frequency*Muscle pair, and
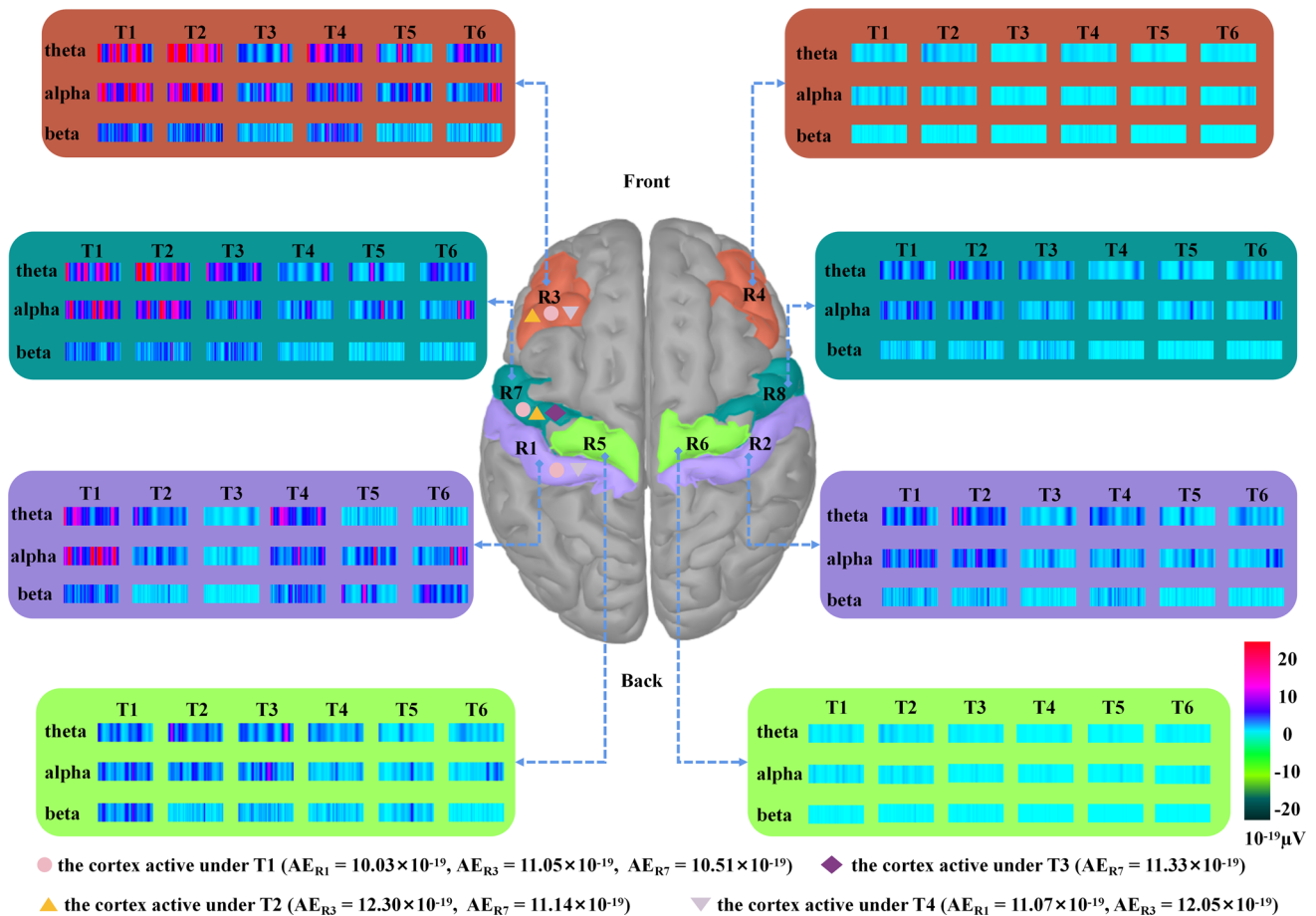
Fig. 2 The averaged time–frequency spectrum of the neurons of the eight ROIs at theta, alpha, and beta frequency bands after source estimations. Time series of the eight ROIs were extracted after EEG source imaging, and time–frequency analysis was performed on the time series of each of the eight ROIs. The time–frequency analyses were averaged across subjects. The time scale of the time–frequency analysis is 5 s. The averaged time–frequency plots of the brain regions connected by arrows are shown in the rectangular boxes for different tasks (T1, T2, T3, T4, T5, T6) and different frequency bands (theta, alpha, beta). The brain regions connected by the matrices in the first, second, third, and fourth panels on the left are R3, R7, R1, and R5, respectively; the brain regions connected by the matrices in the first, second, third, and fourth panels on the right are R4, R8, R2, and R6, respectively. The averaged time–frequency maps represent the dynamic changes of the energy of the three frequency bands of the ROIs over time under different tasks. In this paper, the mean energy value at the frequency band on the time scale is used to measure the level of cortical activation at that frequency band

no significant interaction between the three factors, shown in Table 2.

The number of muscle pairs with coherence coefficients significantly higher than 0.5 ($ps < 0.05$) was largest at the lh band among the four frequency bands and smallest at the beta band. The coherence coefficients of muscles at the lh band are shown in Table 3. The degree of muscle synchronous coupling at the lh band was higher than those at the other three frequency bands (theta, alpha, beta). For example, at the lh band, the coherence coefficients of the four muscles under MO (T1, T2) and MI (T5, T6) were significantly higher than 0.5 ($ps < 0.05$). Four muscles were synchronously coupled at the lh band under MO and MI. Among these three movement conditions, the synchronous coupling of muscles was highest under MO. Under MI, only the left fist-related tasks had a pair of

muscles (B2-B3, right ED-left FCU) with a coherence coefficient significantly higher than 0.5 at the theta band.

Under six tasks, the coherence coefficients between the power spectra of EEG and EMG at six cortico-muscular bands are shown in Fig. 6. The $7 \times 6 \times 32$ ANOVA with the factors Mode, Frequency, and Cortical muscle pair indicated a significant main effect of Mode, the significant main effect of Frequency, the significant main effect of Cortical muscle pair, a significant interaction between the two of the factors, Mode*Frequency, Frequency*Cortical muscle pair, no significant interaction between the other two of the factors Mode*Cortical muscle pair, and no significant interaction between the three factors, shown in Table 4.

At the cortico-muscular theta-lh and theta-theta bands, there was no synchronous coupling (coherence
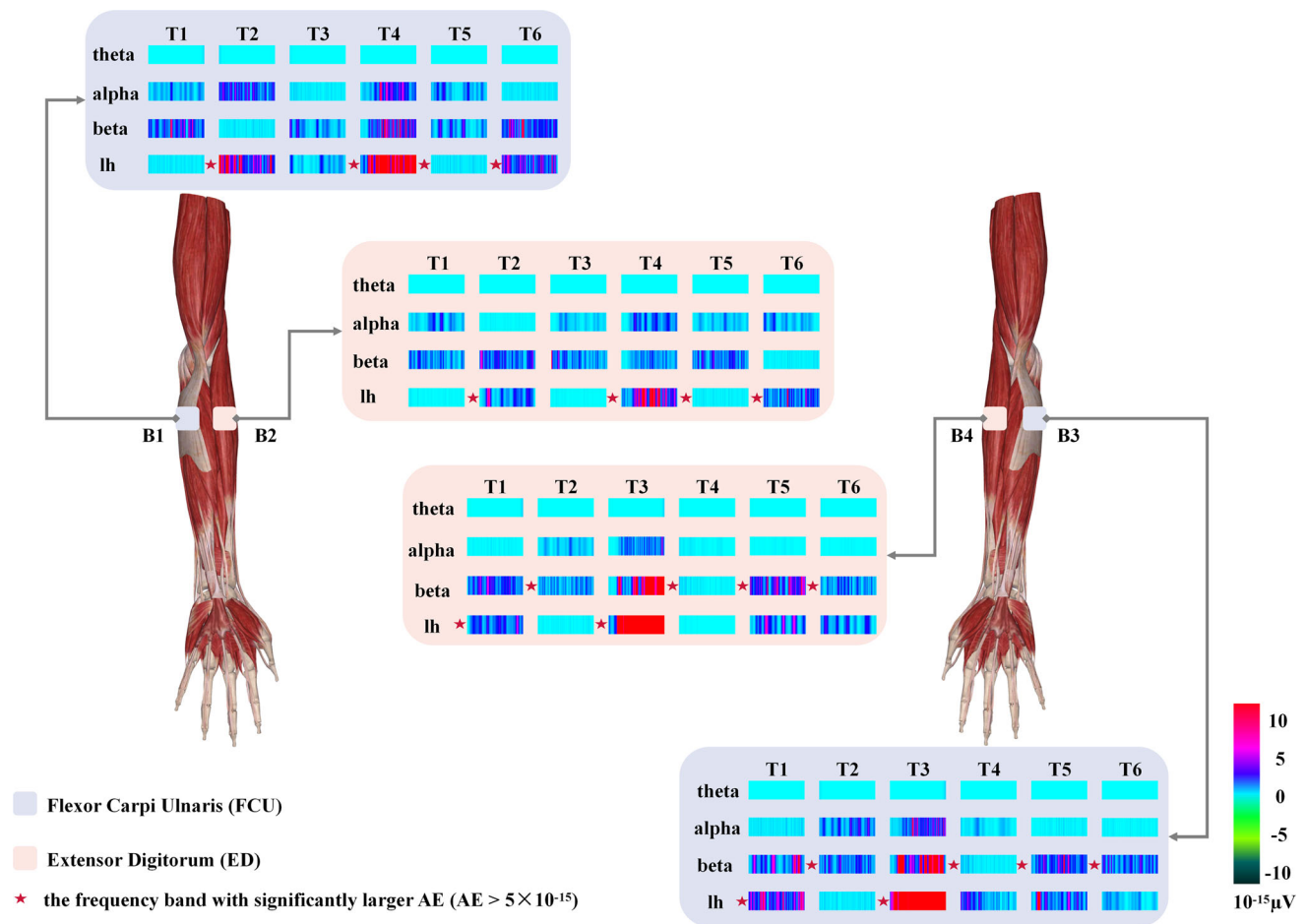
Fig. 3 The averaged time–frequency analysis of EMG signals under MO (T1, T2), ME (T3, T4), and MI tasks (T5, T6) at theta, alpha, beta, and lh bands. The time scale of the time–frequency analyses is 5-s. The time–frequency analysis of EMG signals on different muscles (FCU muscles, ED muscles) were performed and averaged across different subjects. The averaged time–frequency plots represent the energy dynamics at the four frequency bands of the muscles over time for different tasks. The mean energy value at the frequency band on the time scale quantifies the level of muscle activation at that frequency band

coefficients < 0.5) between the activities of neurons in eight ROIs and the electrical activities on the four muscle surfaces.

Although there was a synchronous coupling between cortex and muscle at cortico-muscular alpha-theta and beta-theta bands (coherence coefficients > 0.5) under T2, T3, and T4, there was no statistical significance compared to the Rest condition ($ps > 0.05$). The number of coherence coefficients significantly higher than 0.5 ($ps < 0.05$) between cortices and muscles at the cortico-muscular beta-lh band was the largest. In addition, the coupling degree between cortex and muscle is significantly highest at the cortico-muscular beta-lh band ($p < 0.01$).

The muscles with significant coherence with cortical ROIs under each task are shown in Fig. 7.

It could be seen that the synchronous coupling degree between muscle and cortex was higher at cortico-muscular alpha-lh and beta-lh bands than those at other bands.

(1) At cortico-muscular alpha-lh band. Under T1, T2, T3, T4, 75%, 50%, 62.5%, and 83.3% of the muscles with the significantly highest degree of synchronous coupling in ROIs were on the contralateral forearm, respectively. However, under T5 and T6, 82.5% and 62.5% of ROIs had the significantly highest coherence coefficient with muscles on the ipsilateral forearm, respectively.

(2) At cortico-muscular beta-lh band. Under MO tasks (T1, T2), 75% of the muscles with the significantly highest degree of synchronous coupling in ROIs were on the contralateral forearm. For example, under T1, the significantly highest coherence between R1 of the left hemisphere was B1 on the right forearm. Under ME tasks (T3, T4), 75% and 62.5% of the muscles with the significantly highest synchronous coupling in ROIs were contralateral. Under MI tasks (T5, T6), 75% and 62.5% of the muscles with the significantly highest degree of
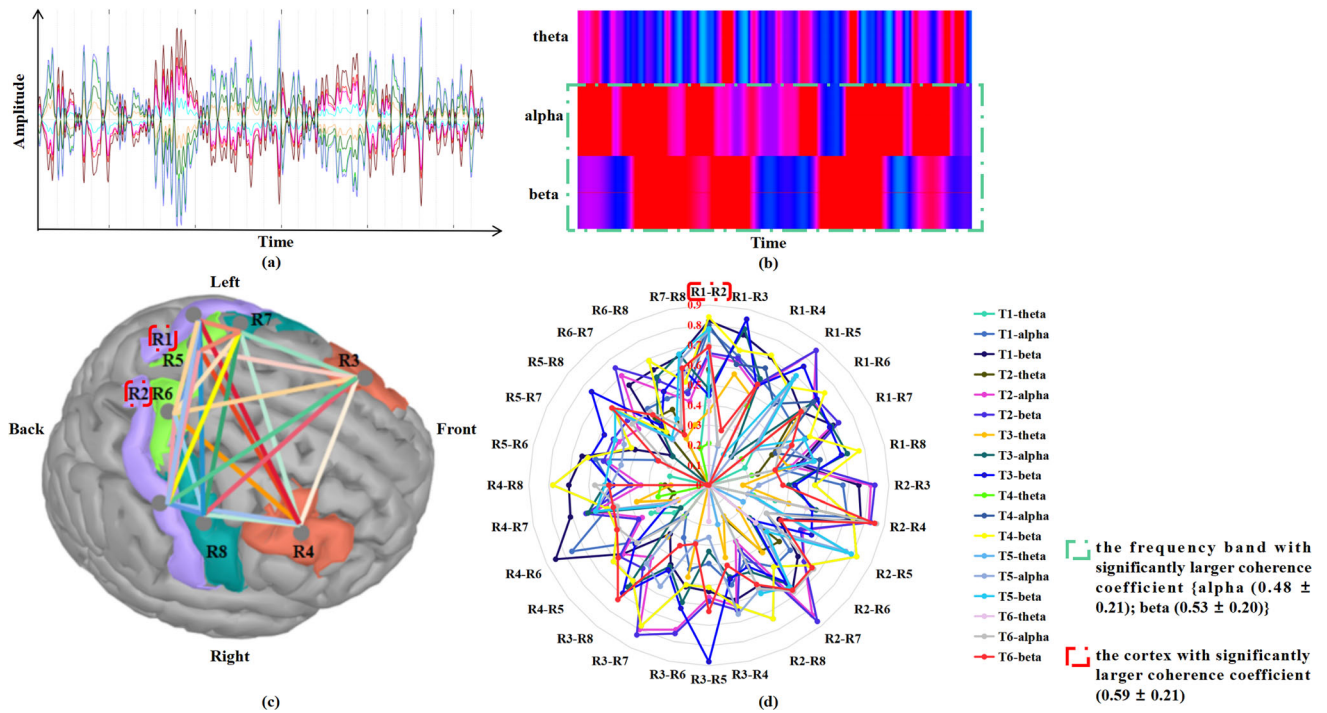
Fig. 4 Time series, time–frequency maps, and coherence between cortices. **a** Time series of ROIs. The time series were extracted from each of the ROIs. **b** Time–frequency map of ROIs. Time–frequency analysis of time series within the brain region of interest were performed at three frequency bands (theta, alpha, beta). **c** Schematic representation of the connections between any two of the eight ROIs. **d** The averaged coherence of three frequency bands (theta, alpha, beta) in the eight ROIs under MO (T1, T2), ME (T3, T4), and MI tasks (T5, T6). The coherence of time–frequency features between any two of the eight ROIs was calculated and averaged across subjects

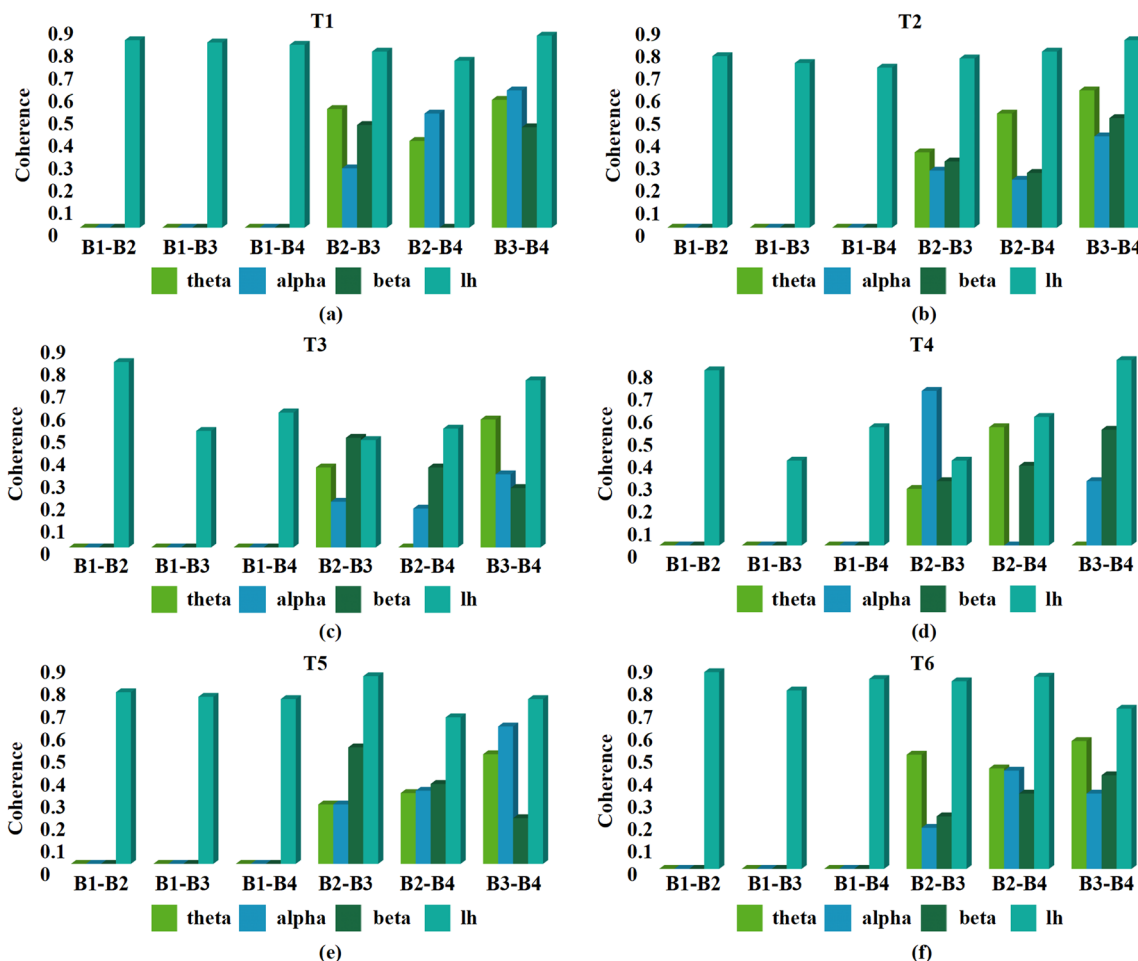**Table 1** The results of ANOVA with the factors Mode, Frequency, and Cortical pair

Source	Assumed Degrees of Freedom	Error Degrees of Freedom	F	p	Partial η^2
Mode	6	4	10.5	< 0.001	0.54
Frequency	2	4	9.75	0.03	0.53
Cortical pair	27	4	2.22	0.01	0.33
Mode*frequency	12	4	5.72	0.01	0.42
Mode*cortical pair	162	4	5.08	0.02	0.41
Frequency*cortical pair	54	4	1.66	< 0.001	0.32
Mode*frequency*cortical pair	323	4	1.57	< 0.001	0.32

synchronous coupling in ROIs were ipsilateral. For example, under T5, the highest coherence between R2 of the right hemisphere was the B1 on the right forearm.

Discussion

The main statistical method used in this paper was multi-factor ANOVA. For post hoc tests, the probability of making a Type I error increases considerably as the number of tests increases. In the pairwise comparisons of inter-cortical, intermuscular, and cortical-muscular coherences at different frequencies, the Type I errors were 14.26%, 18.54%, and 26.49%, respectively. Bonferroni correction was used to adjust significance for pairwise comparisons, making Type I errors less than 0.05. The adjusted significances were 0.0166, 0.0125, and 0.0083 for pairwise comparisons of intercortical, intermuscular, and cortical-muscular coherences.

Fig. 5 The averaged coherence of four frequency bands (lh, theta, alpha, beta) in the four EMG channels under T1 (**a**), T2 (**b**), T3 (**c**), T4 (**d**), T5 (**e**), and T6 (**f**). The coherence of time–frequency features between any two of the four EMG channels was calculated and averaged across subjects. A larger coherence value between two channels indicates a higher probability that both channels are activated simultaneously under the same task

Table 2 The results of ANOVA with the factors Mode, Frequency, and Muscle pair

Source	Assumed Degrees of Freedom	Error Degrees of Freedom	F	p	Partial η^2
Mode	6	3	7.25	0.03	0.43
Frequency	3	3	8.22	< 0.001	0.65
Muscle pair	5	3	7.33	< 0.001	0.45
Mode*frequency	18	3	4.02	0.02	0.31
Mode*muscle pair	30	3	1.64	0.03	0.11
Frequency*muscle pair	15	3	4.64	< 0.001	0.35
Mode*frequency*muscle pair	90	3	0.98	0.61	0.03

The coherence of EEG-EEG

Under the same task, the interaction of frequency bands and cortical pairs affects coherence. For the same cortical pair, the coherence varies across frequency bands. The coherence coefficient is most strongly correlated with the beta frequency band, followed by the alpha frequency band, and finally, the theta frequency band. Researches have shown that alpha and beta frequency bands are motion-related frequency bands (Chholak et al. 2019; Jahangiri and Sepulveda 2019; Neuper and Pfurtscheller 2001; Pfurtscheller 1992). So, it is reasonable for the

Table 3 The coherence coefficients of muscles at the lh band

Task	Muscle pair	Coherence
T1/T2/T3/T4/T5/T6	B1–B2	0.82/0.75/0.81/0.68/0.75/0.86
T1/T2/T3/T4/T5/T6	B1–B3	0.81/0.72/0.51/0.33/0.73/0.78
T1/T2/T3/T4/T5/T6	B1–B4	0.80/0.70/0.59/0.46/0.72/0.83
T1/T2/T3/T4/T5/T6	B2–B3	0.77/0.74/0.47/0.33/0.82/0.82
T1/T2/T3/T4/T5/T6	B2–B4	0.73/0.77/0.52/0.5/0.64/0.84
T1/T2/T3/T4/T5/T6	B3–B4	0.84/0.82/0.73/0.72/0.72/0.70

higher degree of synchronous coupling of cortical pairs at the alpha and beta bands than at theta band. Theta rhythm has been associated with working memory load and attention functions in cognitive-motor tasks (Gevins et al. 1997; Jensen and Tesche 2002). The intensity of the theta band activities has been correlated with task difficulty (Gevins et al. 1997). Our task (i.e., simple daily action) difficulty level is low, requiring lower working memory load and attention, resulting in a lower intensity of theta band activities (Classen et al. 1998; Hummel and Gerloff 2005).

Our results show that the brain regions recruited by right-fist-related tasks were similar among different subjects, while those recruited by left-fist-related tasks were quite different. Such difference may be caused by the difference in proficiency between the dominant hand and the non-dominant hand. Studies have found a strong correlation between hand preference and asymmetries in motor proficiency (Bishop 1989; Triggs et al. 2000). In our study, as all our subjects are right-handed, we postulate that their proficiency in right-hand-related tasks (T2/T4/T6) may be higher than that in left-hand-related tasks (T1/T3/T5), which may lead to the differences in the similarity of brain regions recruited for the task among subjects. Studies have shown that proficiency of actions dramatically influences the functional organization of task-related networks during MO and ME (Amoruso et al. 2017; Weber and Doppelmayr 2016). Under the action-related tasks with high proficiency, the activated brain regions among different subjects were similar. However, there were significant differences in the action-related tasks with low proficiency in the activated brain regions among different subjects. This may help explain why there were more synchronously coupled brain regions in the average analysis under right-fist-related tasks than that under left-fist-related tasks.

Our results also show that the numbers of brain regions recruited by the left-fist and right-fist related tasks were similar in MI. It has been reported that MI's neural mechanisms may differ from those of MO and ME (Hardwick et al. 2018). Our results on this similarity of

results in the MI tasks may be because the brain regions recruited by MI may not be affected by motion proficiency.
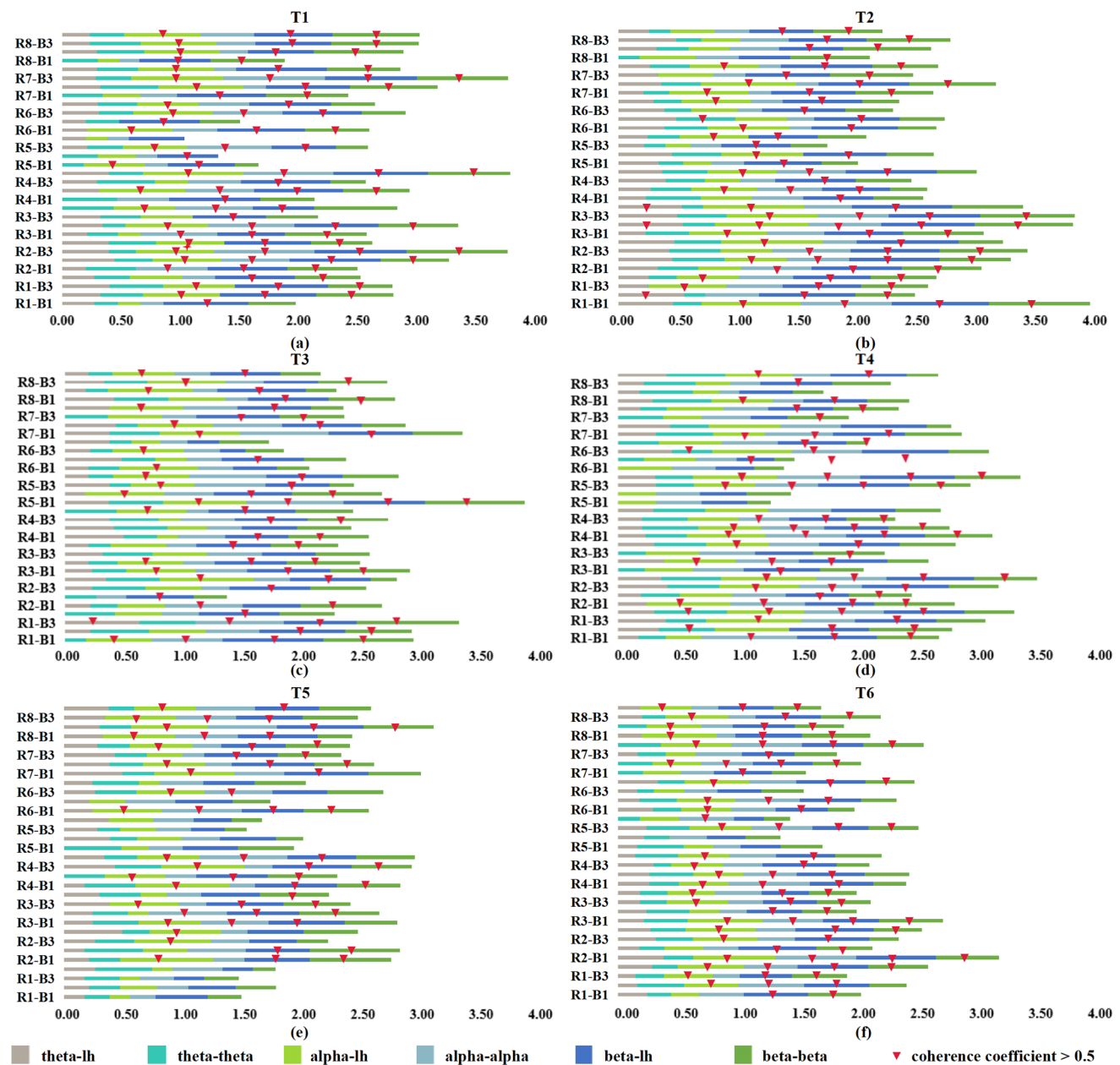
The coherence of EMG-EMG

From the results of EMG-EMG coherence, the synchronous coupling degree between muscles was the highest at the lh band. In this paper, the lh band was chosen at the frequency band with task-related maximum energy density. The components of muscle activity in healthy individuals are more concentrated on the frequencies with maximum activity energy (Politti et al. 2016), which may explain the higher degree of synchronous coupling at the lh band than at others for muscle activities. The components in the EMG signal below 20 Hz contain noise and do not contain reliable information (De Luca et al. 2010). Studies have shown that the components of EMG signals below 100 Hz can reflect modulation of the motor neuron pool, which modifies the voluntary effort (Christou & Neto 2010; Neto et al. 2010). Moreover, most power in the interference EMG signal occurs at higher frequencies (above 100 Hz) (Christou and Neto 2010). The EMG signal components at the lh band (30–100 Hz) can provide reliable information related to motion. In the future, we will use other methods (Andrade et al. 2006) to further validate the effectiveness of our bands.

The coherence of EEG-EMG

The time–frequency coherence of EEG-EMG

Both the frequency band and the interaction of the frequency bands and muscle pairs have an effect on the coherence. The strongest cortico-muscular coherence is found at the beta-lh band. Consistent with other studies, frequency is an important factor affecting cortico-muscular coherence (Liu et al. 2019). Studies on cortico-muscular coherence suggested that cortical and electrical muscle activity are co-frequent (i.e., beta, gamma bands) under motor tasks (Gwin and Ferris 2012; Riddle and Baker 2005). However, our findings differ from those in that cortico-muscular coherence is strongest at the different frequency bands where their respective electrical activities are most active. The electrical activity of cortices (beta) and muscles (lh) may be at different frequencies under motor tasks. The frequency of cortical activity was the same as in the previous study, while the frequency of electrical muscle activity was different from the previous study (Gwin and Ferris 2012; Riddle and Baker 2005). As discussed above regarding lh band selection, the higher and lower ends of this band agree well with the results of the current studies based on EMG signals (De Luca et al. 2010; Christou and Neto 2010). In addition, the lh band is where

Fig. 6 The averaged coherence between EEG of 8 ROIs (R1, R2, R3, R4, R5, R6, R7, R8) and EMG of 4 channels (B1, B2, B3, B4) under T1 (**a**), T2 (**b**), T3 (**c**), T4 (**d**), T5 (**e**), and T6 (**f**). The coherence of time–frequency features between each region of the eight ROIs and each channel of the four EMG channels was calculated and averaged across subjects. A larger coherence value between cortex and muscle indicates a stronger functional connection between that cortex and that muscle, and that pathway may exist between that cortex and muscle for information exchange. Coherence coefficients less than 0.5 are not marked with numbers. * $p < 0.05$

the active energy is concentrated and is most relevant to the components of muscle activity (Politti et al. 2016). These may account for the highest degree of synchronous coupling of muscle activity components at the lh band with cortical activity components at the beta band.

As mentioned before, unlike previous studies (Dal Maso et al. 2017; Nijhuis et al. 2021), we did not use scalp potentials directly but projected scalp potentials to the cerebral cortex by traceability technique (Michel and Brunet 2019). We explored the spatial coherence between cortex and muscle, requiring higher precision for the cortex's location. Therefore, we projected scalp potentials to the cerebral cortex to obtain a more precise location, rather than inferring the location of the cortex corresponding to the electrode directly from the location of the electrode where the scalp potential was recorded.

We then calculated the coherence between brain source activity in the cerebral cortex and electrical activity on the

Table 4 The results of ANOVA with the factors Mode, Frequency, and Cortical muscle pair

Source	Assumed Degrees of Freedom	Error Degrees of Freedom	F	p	Partial η^2
Mode	6	3	9.7	0.001	0.69
Frequency	5	3	7.73	< 0.001	0.55
Cortical muscle Pair	31	3	5.09	< 0.001	0.45
Mode*frequency	30	3	3.43	0.03	0.33
Mode*cortical Muscle Pair	186	3	3.72	0.15	0.17
Frequency*cortical Muscle Pair	155	3	1.97	0.02	0.11
Mode*frequency*cortical Muscle Pair	930	3	1.65	0.38	0.08

muscle surface. The electrodes of EMG in this study were placed on the forearm muscles (Hedt et al. 2020), different from those in previous studies in which the electrodes were put on the hand. These differences between our studies and previous studies may help explain why our results are different from theirs.
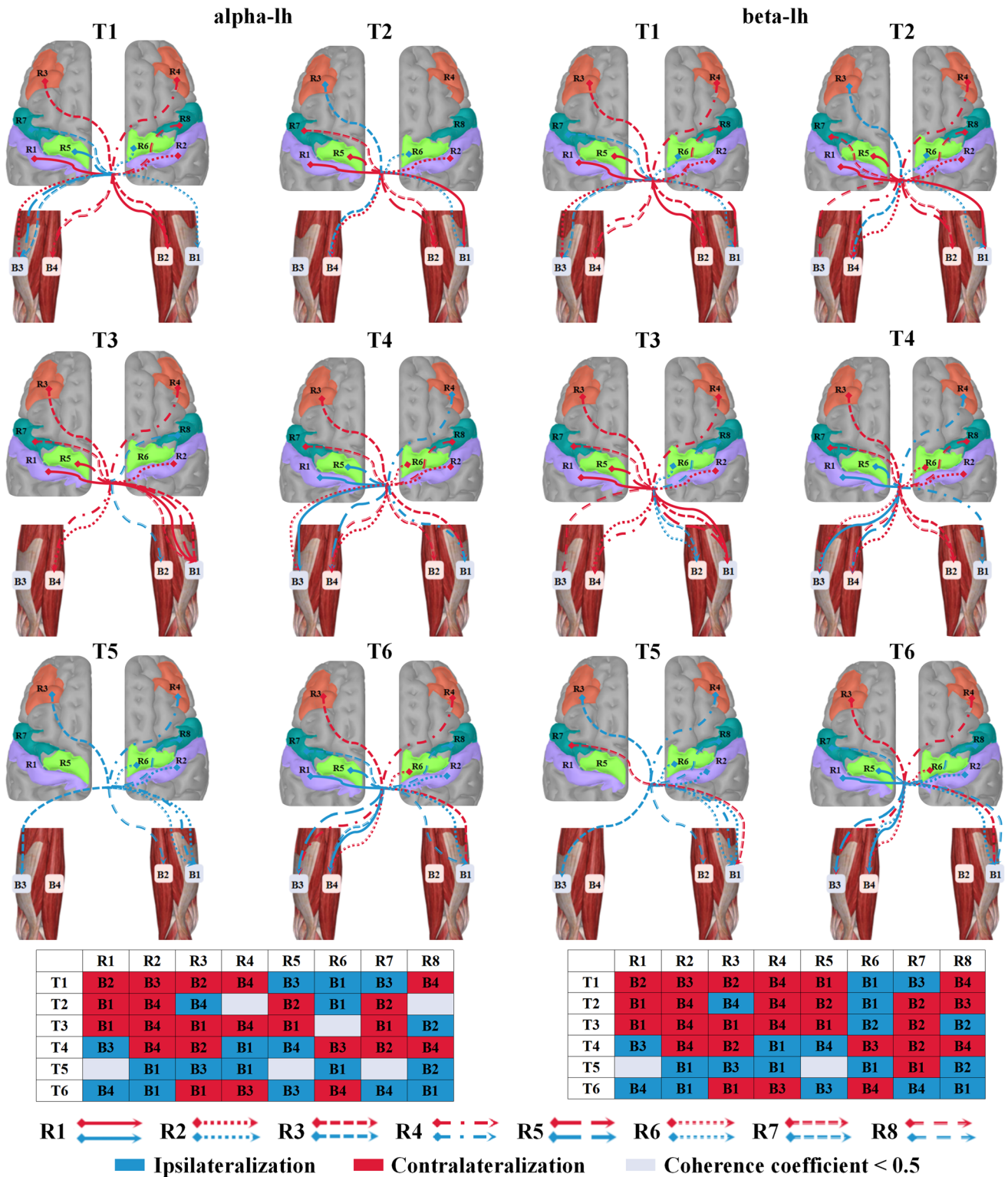
The spatial coherence of EEG-EMG

To the best of our knowledge, there is no research to investigate the similarities and differences in time–frequency and spatial coherence between cortex and muscle under these three motor conditions (MO, ME, MI). We analyzed the spatial characteristics under three movement conditions based on the coherence between electrical activities in the cortex and those on the muscle surface using source imaging techniques. Then, we calculated the source estimations of the M1, DLPEC, SMA, and PMC.

The M1, DLPEC, SMA, and PMC of the contralateral and ipsilateral hemispheres are selectively involved in MO, ME, and MI. Our results show that these cortices can be responsible for the tasks of the contralateral and ipsilateral fist tasks, and that the contralateral and ipsilateral cortices are recruited for each unilateral hand task. These results agree with results in literature that the SMA, M1, PMC, and DLPFC cortex control contralateral and ipsilateral hand movements (Nakayama et al. 2015) (Porro et al. 2000) (Gallivan et al. 2013).

Our results show that synchronous coupling between cortex and muscle has a contralateral advantage under MO and ME, which is in accordance with previous studies. Studies have reported that the activation of the contralateral motor areas can be observed when performing the prominent-handed movement (Baker and Baker 2003; Tun et al. 2021). Clinical studies observed that the contralateral hand of the damaged hemisphere show paralysis symptoms in stroke patients (Farmer et al. 1993). It has been demonstrated that ME and MO are functionally intertwined and share common underlying neural networks (Montagna et al. 2005; Mukamel et al. 2010). MO forms an interaction

between ME and visual perception, which provides a solid foundation for imitation, action understanding, and motor learning (Heiser et al. 2003; Stefan et al. 2005). MO usually induces selective regulation of corticospinal projections, which increases contralateral cortical motor evoked potentials (Gueugneau et al. 2016). Also, it has been proved that during ME of unilateral hand movement, involuntary mirror movements may occur in the contralateral resting homologous muscles. In order to prevent mirror movements, the contralateral PMC of the active hand will have an inhibitory effect on the ipsilateral PMC (Morishita et al. 2012; Talelli et al. 2008). Our results suggest that the PMC, SMA, M1, and DLPFC may also be involved in inhibiting mirror movements. These reasons may lead to the contralateral advantage of the coherence between cortex and muscle in the MO and ME tasks related to fists.

Our results suggest that the cortico-muscular synchronous coupling has the ipsilateralization advantage during MI. At present, there is no unified conclusion on the function of the bilateral cortex during MI. During MI, the event-related desynchronization (ERD), which reflects motor cortical excitability, was observed in the contralateral M1 and SMA (Takemi et al. 2015, 2013). These studies did not directly explore the coherence between cortex and muscle but explored the relationship between cortex and muscle by analyzing the changes of ERD and motor-related potentials under transcranial magnetic stimulation (TMS). EEGs of most of these subjects were recorded from a few channels over the contralateral SMA due to the inconvenience of using TMS, thus, results from these few EEG channels may not be able to show the whole information in the brain during the experiments. Our results showed that MI stimulated greater ipsilateral cortical activation, such as PMC and SMA, which is in consonance with previous fMRI studies (Porro et al. 2000; Ueno et al. 2010). The process of MI includes the generation, maintenance, and operation of motion-related images (Bello et al. 2020). In these psychological processes, the

Fig. 7 The spatial coherence of EEG-EMG under MO (T1, T2), ME (T3, T4), and MI tasks (T5, T6). The left and right views show the cortical-muscle pairs with the highest coherence under each task at the cortico-muscular alpha-lh band and the cortico-muscular beta-lh band, respectively. The presence of lines connecting the cortex to the muscle suggests that there may be pathways for information exchange between the cortex and the muscle. Different line patterns were used to differentiate connections from different brain regions to muscles

activation of ipsilateral cortices may be related to movement, cognition, and perception.

Our findings suggest that PMC, DLPEC, SMA, and M1 of bilateral hemispheres are the specific regions of MO, ME, and MI. Bilateral cortices are involved in the three motor conditions, but their pathways of regulating muscles are different. Under MO and ME, the synchronous coupling between muscle and cortex presents a contralateral advantage, but under the condition of MI, the synchronous coupling between muscle and cortex presents an ipsilateral advantage.

There are some limitations to this study. First, this study created areas according to the brain atlas commonly used in literature. However, the size of areas is not small enough, so the positioning resolution of brain regions responsible for regulating muscles may be limited. Future studies may divide brain regions into smaller areas to improve the spatial resolution of coherence between EEG and EMG. Secondly, the number of EMG electrodes is small, covering a few muscle groups. This may result in some task-related muscles not being found. In the future, we will use tiny EMG electrode arrays to cover more muscles. Third, all our subjects were right-handed, thus our results yielded from these experiments may not representative for the left-handed population. Whether these results are similar to the left-hand population is not known yet due to unavailability. More studies will be needed in the future.

Conclusion

In this study, we analyzed and compared the cortico-muscular coherence of time–frequency and spatial characteristics among MO, ME, and MI. For time–frequency characteristics, the cortico-muscular coherence was strongest at the beta-lh band. MO and ME had a contralateral advantage while MI had an ipsilateral advantage for spatial characteristics. Our results suggest that the cortico-muscular beta-lh band is critical for the synchronous coupling of cortex and muscle. Furthermore, our findings show that M1, DLPFC, SMA and PMC are involved in MO, ME and MI, but these cortices regulate muscles in different pathways under different motor conditions. These findings provide novel insights into the mechanisms of motor function rehabilitation and stroke treatment.

Declarations

Conflict of interest None.

References

Amoruso L, Ibanez A, Fonseca B, Gadea S, Sedeno L, Sigman M, Fraiman D (2017) Variability in functional brain networks predicts expertise during action observation. Neuroimage 146:690–700. https://doi.org/10.1016/j.neuroimage.2016.09.041

Andrade AO, Nasuto S, Kyberd P, Sweeney-Reed CM, Van Kanijn FR (2006) EMG signal filtering based on empirical mode decomposition. Biomed Signal Process Control 1(1):44–55. https://doi.org/10.1016/j.bspc.2006.03.003

Andrews AP, Atler KE, Portz JD, VanPuymbroeck M, Rose CM, Schmid AA (2021) Occupational therapists' use of yoga in post-stroke care: a descriptive qualitative study. Br J Occup Ther 84(4):240–250. https://doi.org/10.1177/0308022620910371

Baccetto SL, Lehmann C (2019) Microcirculatory changes in experimental models of stroke and CNS-injury induced immunodepression. Int J Mol Sci. https://doi.org/10.3390/ijms20205184

Baker MR, Baker SN (2003) The effect of diazepam on motor cortical oscillations and corticomuscular coherence studied in man. J Physiol 546(3):931–942. https://doi.org/10.1113/jphysiol.2002.029553

Bello UM, Winser SJ, Chan CCH (2020) Role of kinaesthetic motor imagery in mirror-induced visual illusion as intervention in post-stroke rehabilitation. Rev Neurosci 31(6):659–674. https://doi.org/10.1515/revneuro-2019-0106

Bishop DV (1989) Does hand proficiency determine hand preference? Br J Psychol 80(Pt 2):191–199. https://doi.org/10.1111/j.2044-8295.1989.tb02313.x

Chholak P, Niso G, Maksimenko VA, Kurkin SA, Frolov NS, Pitsik EN, Pisarchik AN (2019) Visual and kinesthetic modes affect motor imagery classification in untrained subjects. Sci Rep. https://doi.org/10.1038/s41598-019-46310-9

Christou E, Neto O (2010) Identification of oscillations in muscle activity from surface EMG: reply to halliday and farmer. J Neurophysiol 103(6):3548–3549. https://doi.org/10.1152/jn.00325.2010

Classen J, Gerloff C, Honda M, Hallett M (1998) Integrative visuomotor behavior is associated with interregionally coherent oscillations in the human brain. J Neurophysiol 79(3):1567–1573. https://doi.org/10.1152/jn.1998.79.3.1567

Collins DL, Zijdenbos AP, Kollokian V, Sled JG, Kabani NJ, Holmes CJ, Evans AC (1998) Design and construction of a realistic digital brain phantom. IEEE Trans Med Imaging 17(3):463–468. https://doi.org/10.1109/42.712135

Dal Maso F, Longcamp M, Cremoux S, Amarantini D (2017) Effect of training status on beta-range corticomuscular coherence in agonist vs. antagonist muscles during isometric knee contractions. Exp Brain Res 235(10):3023–3031. https://doi.org/10.1007/s00221-017-5035-z

Dale AM, Sereno MI (1993) Improved localization of cortical activity by combining EEG and MEG with MRI cortical surface reconstruction - a linear-approach. J Cogn Neurosci 5(2):162–176. https://doi.org/10.1162/jocn.1993.5.2.162

De Luca CJ, Gilmore LD, Kuznetsov M, Roy SH (2010) Filtering the surface EMG signal: movement artifact and baseline noise contamination. J Biomech 43(8):1573–1579

Di Nota PM, Chartrand JM, Levkov GR, Montefusco-Siegmund R, DeSouza JFX (2017) Experience-dependent modulation of alpha and beta during action observation and motor imagery. BMC Neurosci. https://doi.org/10.1186/s12868-017-0349-0

Farmer SF, Bremner FD, Halliday DM, Rosenberg JR, Stephens JA (1993) The frequency content of common synaptic inputs to mononeurones studied during voluntary isometric contraction in man. J Physiol 470:127–155. https://doi.org/10.1113/jphysiol.1993.sp019851

Feigin VL, Forouzanfar MH, Krishnamurthi R, Mensah GA, Connor M, Bennett DA, Grp GBDSE (2014) Global and regional burden of stroke during 1990–2010: findings from the Global Burden of Disease Study 2010. Lancet 383(9913):245–255. https://doi.org/10.1016/s0140-6736(13)61953-4

Foong R, Ang KK, Quek C, Guan C, Phua KS, Kuah CWK, Deshmukh VA, Yam LHL, Rajeswaran DK, Tang N, Chew E (2019) Assessment of the efficacy of EEG-based MI-BCI with visual feedback and EEG correlates of mental fatigue for upper-limb stroke rehabilitation. IEEE Trans Biomed Eng 67(3):786–795

Gallivan JP, McLean DA, Flanagan JR, Culham JC (2013) Where one hand meets the other: limb-specific and action-dependent movement plans decoded from preparatory signals in single human frontoparietal brain areas. J Neurosci 33(5):1991-2008A. https://doi.org/10.1523/jneurosci.0541-12.2013

Gao JF, Yang Y, Sun JC, Yu G (2010) Automatic removal of various artifacts from EEG signals using combined methods. J Clin Neurophysiol 27(5):312–320. https://doi.org/10.1097/WNP.0b013e3181f534f4

Gao YY, Ren LL, Li RH, Zhang YC (2018) Electroencephalogram-electromyography coupling analysis in stroke based on symbolic transfer entropy. Front Neurol. https://doi.org/10.3389/fneur.2017.00716

Garcia-Cabo C, Lopez-Cancio E (2020) Exercise and stroke. In: Xiao J (Ed) Physical exercise for human health (Vol. 1228, pp. 195–203)

Garrison KA, Aziz-Zadeh L, Wong SW, Liew SL, Winstein CJ (2013) Modulating the motor system by action observation after stroke. Stroke 44(8):2247–2253. https://doi.org/10.1161/Strokeaha.113.001105

Gevins A, Smith ME, McEvoy L, Yu D (1997) High-resolution EEG mapping of cortical activation related to working memory: effects of task difficulty, type of processing, and practice. Cereb Cortex 7(4):374–385. https://doi.org/10.1093/cercor/7.4.374

Gueugneau N, Bove M, Ballay Y, Papaxanthis C (2016) Interhemispheric inhibition is dynamically regulated during action observation. Cortex 78:138–149. https://doi.org/10.1016/j.cortex.2016.03.003

Guillot A, Collet C, Nguyen VA, Malouin F, Richards C, Doyon J (2008) Functional neuroanatomical networks associated with expertise in motor imagery. Neuroimage 41(4):1471–1483. https://doi.org/10.1016/j.neuroimage.2008.03.042

Gwin JT, Ferris DP (2012) Beta- and gamma-range human lower limb corticomuscular coherence. Front Hum Neurosci. https://doi.org/10.3389/fnhum.2012.00258

Halliday DM, Rosenberg JR, Amjad AM, Breeze P, Conway BA, Farmer SF (1995) A framework for the analysis of mixed time series/point process data - Theory and application to the study of physiological tremor, single motor unit discharges and electromyograms. Prog Biophys Mol Biol 64(2–3):237–278. https://doi.org/10.1016/s0079-6107(96)00009-0

Hanakawa T, Immisch I, Toma K, Dimyan MA, Van Gelderen P, Hallett M (2003) Functional properties of brain areas associated with motor execution and imagery. J Neurophysiol 89(2):989–1002. https://doi.org/10.1152/jn.00132.2002

Hardwick RM, Caspers S, Eickhoff SB, Swinnen SP (2018) Neural correlates of action: Comparing meta-analyses of imagery, observation, and execution. Neurosci Biobehav Rev 94:31–44. https://doi.org/10.1016/j.neubiorev.2018.08.003

Hatem SM, Saussez G, della Faille M, Prist V, Zhang X, Dispa D, Bleyenheuft Y (2016) Rehabilitation of motor function after stroke: a multiple systematic review focused on techniques to stimulate upper extremity recovery. Front Human Neurosci 10:442

Hedt C, Lambert BS, Daum J, Pearson JM, McCulloch PC (2020) Forearm position matters during eccentric shoulder exercises: an EMG recruitment study with implications for rehabilitation. Int J Sports Phys Ther 15(6):1110–1118. https://doi.org/10.26603/ijspt20201110

Heiser M, Iacoboni M, Maeda F, Marcus J, Mazziotta JC (2003) The essential role of Broca's area in imitation. Eur J Neurosci 17(5):1123–1128. https://doi.org/10.1046/j.1460-9568.2003.02530.x

Hsueh YH, Yin C, Chen YH (2015) Hardware system for real-time EMG signal acquisition and separation processing during electrical stimulation. J Med Syst 39(9):1–8

Hummel F, Gerloff C (2005) Larger interregional synchrony is associated with greater behavioral success in a complex sensory integration task in humans. Cereb Cortex 15(5):670–678. https://doi.org/10.1093/cercor/bhh170

Jahangiri A, Sepulveda F (2019) The relative contribution of high-gamma linguistic processing stages of word production, and motor imagery of articulation in class separability of covert speech tasks in EEG data. J Med Syst. https://doi.org/10.1007/s10916-018-1137-9

Jensen O, Tesche CD (2002) Frontal theta activity in humans increases with memory load in a working memory task. Eur J Neurosci 15(8):1395–1399. https://doi.org/10.1046/j.1460-9568.2002.01975.x

Kim B, Kim L, Kim YH, Yoo SK (2017) Cross-association analysis of EEG and EMG signals according to movement intention state. Cogn Syst Res 44:1–9. https://doi.org/10.1016/j.cogsys.2017.02.001

Kleim JA, Jones TA (2008) Principles of experience-dependent neural plasticity: implications for rehabilitation after brain damage. J Speech Lang Hearing Res 51(1):S225-239

Krauth R, Schwertner J, Vogt S, Lindquist S, Sailer M, Sickert A, Sweeney-Reed CM (2019) Cortico-muscular coherence is reduced acutely post-stroke and increases bilaterally during motor recovery: a pilot study. Front Neurol 10:126

Liu AK, Belliveau JW, Dale AM (1998) Spatiotemporal imaging of human brain activity using functional MRI constrained magnetoencephalography data: Monte Carlo simulations. Proc Natl Acad Sci USA 95(15):8945–8950. https://doi.org/10.1073/pnas.95.15.8945

Liu JB, Sheng YX, Liu HH (2019) Corticomuscular coherence and its applications. Front Human Neurosci. https://doi.org/10.3389/fnhum.2019.00100

Luo TT, Wang J, Hao SL, Guo TW, Ren P, Cheng ZJ, Wang BC (2017) Brain drug delivery systems for the stroke intervention and recovery. Curr Pharm Design 23(15):2258–2267. https://doi.org/10.2174/1381612822666161025155058

Michel CM, Brunet D (2019) EEG source imaging: a practical review of the analysis steps. Front Neurol. https://doi.org/10.3389/fneur.2019.00325

Mizuguchi N, Nakamura M, Kanosue K (2017) Task-dependent engagements of the primary visual cortex during kinesthetic and visual motor imagery. Neurosci Lett 636:108–112

Montagna M, Cerri G, Borroni P, Baldissera F (2005) Excitability changes in human corticospinal projections to muscles moving hand and fingers while viewing a reaching and grasping action.

Eur J Neurosci 22(6):1513–1520. https://doi.org/10.1111/j.1460-9568.2005.04336.x

Morishita T, Uehara K, Funase K (2012) Changes in interhemispheric inhibition from active to resting primary motor cortex during a fine-motor manipulation task. J Neurophysiol 107(11):3086–3094. https://doi.org/10.1152/jn.00888.2011

Mukamel R, Ekstrom AD, Kaplan J, Iacoboni M, Fried I (2010) Single-neuron responses in humans during execution and observation of actions. Curr Biol 20(8):750–756. https://doi.org/10.1016/j.cub.2010.02.045

Muthuraman M, Raethjen J, Koirala N, Anwar AR, Mideksa KG, Elble R, Deuschl G (2018) Cerebello-cortical network fingerprints differ between essential, Parkinson's and mimicked tremors. Brain 141:1770–1781. https://doi.org/10.1093/brain/awy098

Naghavi M, Abajobir AA, Abbafati C, Abbas KM, Abd-Allah F, Abera SF, Collaborato GCD (2017) Global, regional, and national age-sex specific mortality for 264 causes of death, 1980–2016: a systematic analysis for the Global Burden of Disease Study 2016. Lancet 390(10100):1151–1210. https://doi.org/10.1016/S0140-6736(17)32152-9

Nakayama Y, Yokoyama O, Hoshi E (2015) Distinct neuronal organizations of the caudal cingulate motor area and supplementary motor area in monkeys for ipsilateral and contralateral hand movements. J Neurophysiol 113(7):2845–2858. https://doi.org/10.1152/jn.00854.2014

Neto OP, Baweja HS, Christou EA (2010) Increased voluntary drive is associated with changes in common oscillations from 13 to 60 Hz of interference but not rectified electromyography. Muscle Nerve 42(3):348–354. https://doi.org/10.1002/mus.21687

Neuper C, Pfurtscheller G (2001) Event-related dynamics of cortical rhythms: frequency-specific features and functional correlates. Int J Psychophysiol 43(1):41–58. https://doi.org/10.1016/s0167-8760(01)00178-7

Nijhuis P, Keller PE, Nozaradan S, Varlet M (2021) Dynamic modulation of cortico-muscular coupling during real and imagined sensorimotor synchronisation. Neuroimage. https://doi.org/10.1016/j.neuroimage.2021.118209

Ono Y, Wada K, Kurata M, Seki N (2018) Enhancement of motor-imagery ability via combined action observation and motor-imagery training with proprioceptive neurofeedback. Neuropsychologia 114:134–142

Pfurtscheller G (1992) Event-related synchronization (ERS) - an electrophysiological correlate of cortical areas at rest. Electroencephalogr Clin Neurophysiol 83(1):62–69. https://doi.org/10.1016/0013-4694(92)90133-3

Politti F, Casellato C, Kalytczak MM, Garcia MBS, Biasotto-Gonzalez DA (2016) Characteristics of EMG frequency bands in temporomandibullar disorders patients. J Electromyogr Kinesiol 31:119–125. https://doi.org/10.1016/j.jelekin.2016.10.006

Porro CA, Cettolo V, Francescato MP, Baraldi P (2000) Ipsilateral involvement of primary motor cortex during motor imagery. Eur J Neurosci 12(8):3059–3063. https://doi.org/10.1046/j.1460-9568.2000.00182.x

Qiu S, Yi WB, Xu JP, Qi HZ, Du JG, Wang CF, Ming D (2016) Event-related beta EEG changes during active, passive movement and functional electrical stimulation of the lower limb. IEEE Trans Neural Syst Rehabil Eng 24(2):283–290. https://doi.org/10.1109/tnsre.2015.2476481

Ramos-Murguialday A, Broetz D, Rea M, Laer L, Yilmaz O, Brasil FL, Birbaumer N (2013) Brain-machine interface in chronic stroke rehabilitation: a controlled study. Ann Neurol 74(1):100–108. https://doi.org/10.1002/ana.23879

Riddle CN, Baker SN (2005) Manipulation of peripheral neural feedback loops alters human corticomuscular coherence.

J Physiol 566(2):625–639. https://doi.org/10.1113/jphysiol.2005.089607

Sakurada T, Nakajima T, Morita M, Hirai M, Watanabe E (2017) Improved motor performance in patients with acute stroke using the optimal individual attentional strategy. Sci Rep. https://doi.org/10.1038/srep40592

Signal NEJ, McLaren R, Rashid U, Vandal A, King M, Almesfer F, Taylor D (2020) Haptic nudges increase affected upper limb movement during inpatient stroke rehabilitation: multiple-period randomized crossover study. Jmir Mhealth Uhealth. https://doi.org/10.2196/17036

Stefan K, Cohen LG, Duque J, Mazzocchio R, Celnik P, Sawaki L, Classen J (2005) Formation of a motor memory by action observation. J Neurosci 25(41):9339–9346. https://doi.org/10.1523/Jneurosci.2282-05.2005

Tadel F, Baillet S, Mosher JC, Pantazis D, Leahy RM (2011) Brainstorm: a user-friendly application for MEG/EEG analysis. Comput Intell Neurosci. https://doi.org/10.1155/2011/879716

Takemi M, Masakado Y, Liu MG, Ushiba J (2013) Event-related desynchronization reflects downregulation of intracortical inhibition in human primary motor cortex. J Neurophysiol 110(5):1158–1166. https://doi.org/10.1152/jn.01092.2012

Takemi M, Masakado Y, Liu M, Ushiba J (2015) Sensorimotor event-related desynchronization represents the excitability of human spinal motoneurons. Neuroscience 297:58–67. https://doi.org/10.1016/j.neuroscience.2015.03.045

Talelli P, Waddingham W, Ewas A, Rothwell JC, Ward NS (2008) The effect of age on task-related modulation of interhemispheric balance. Exp Brain Res 186(1):59–66. https://doi.org/10.1007/s00221-007-1205-8

Triggs WJ, Calvanio R, Levine M, Heaton RK, Heilman KM (2000) Predicting hand preference with performance on motor tasks. Cortex 36(5):679–689. https://doi.org/10.1016/s0010-9452(08)70545-8

Tun NN, Sanuki F, Iramina K (2021) Electroencephalogram-electromyogram functional coupling and delay time change based on motor task performance. Sensors. https://doi.org/10.3390/s21134380

Tuncel D, Dizibuyuk A, Kiymik MK (2010) Time frequency based coherence analysis between EEG and EMG activities in fatigue duration. J Med Syst 34(2):131–138. https://doi.org/10.1007/s10916-008-9224-y

Ueno T, Inoue M, Matsuoka T, Abe T, Maeda H, Morita K (2010) Comparison between a real sequential finger and imagery movements: An fMRI study revisited. Brain Imaging Behav 4(1):80–85. https://doi.org/10.1007/s11682-009-9087-y

von Ellenrieder N, Muravchik CH, Nehorai A (2005) A meshless method for solving the EEG forward problem. IEEE Trans Biomed Eng 52(2):249–257. https://doi.org/10.1109/tbme.2004.840499

Weber E, Doppelmayr M (2016) Kinesthetic motor imagery training modulates frontal midline theta during imagination of a dart throw. Int J Psychophysiol 110:137–145. https://doi.org/10.1016/j.ijpsycho.2016.11.002

Zhang QH, Zhang P, Song L, Yang Y, Yuan S, Chen YX, Bai XJ (2019) Brain activation of elite race walkers in action observation, motor imagery, and motor execution tasks: a pilot study. Front Human Neurosci. https://doi.org/10.3389/fnhum.2019.00080

Zhang XD, Li HZ, Lu ZF, Yin G (2021) Homology characteristics of EEG and EMG for lower limb voluntary movement intention. Front Neurorobot. https://doi.org/10.3389/fnbot.2021.642607

Zhao XG, Chu YQ, Han JD, Zhang ZQ (2016) SSVEP-based brain-computer interface controlled functional electrical stimulation system for upper extremity rehabilitation. IEEE Trans Syst Man

Cybern Syst 46(7):947–956. https://doi.org/10.1109/tsmc.2016.2523762

Zulauf-Czaja A, Al-Taleb MKH, Purcell M, Petric-Gray N, Cloughley J, Vuckovic A (2021) On the way home: a BCI-FES hand therapy self-managed by sub-acute SCI participants and their caregivers: a usability study. J Neuroeng Rehabil. https://doi.org/10.1186/s12984-021-00838-y